

Antiferromagnetism in the Hubbard Model on the Bernal-Stacked Honeycomb Bilayer

Thomas C. Lang,^{1,2,3,*} Zi Yang Meng,⁴ Michael M. Scherer,^{1,3} Stefan Uebelacker,^{1,3}
Fakher F. Assaad,⁵ Alejandro Muramatsu,⁶ Carsten Honerkamp,^{1,3} and Stefan Wessel^{1,2,3}

¹*Institute for Theoretical Solid State Physics, RWTH Aachen University, Aachen, Germany*

²*JARA-HPC High Performance Computing*

³*JARA-FIT Fundamentals of Future Information Technology*

⁴*Center for Computation and Technology, Louisiana State University, Baton Rouge, Louisiana 70803, USA*

⁵*Institute for Theoretical Physics and Astrophysics, University of Würzburg, Würzburg, Germany*

⁶*Institut für Theoretische Physik III, University of Stuttgart, Stuttgart, Germany*

Using a combination of quantum Monte Carlo simulations, functional renormalization group calculations and mean-field theory, we study the Hubbard model on the Bernal-stacked honeycomb bilayer at half-filling as a model system for bilayer graphene. The free bands consisting of two Fermi points with quadratic dispersions lead to a finite density of states at the Fermi level, which triggers an antiferromagnetic instability that spontaneously breaks sublattice and spin rotational symmetry once local Coulomb repulsions are introduced. Our results reveal an inhomogeneous participation of the spin moments in the ordered ground state, with enhanced moments at the threefold coordinated sites. Furthermore, we find the antiferromagnetic ground state to be robust with respect to enhanced interlayer couplings and extended Coulomb interactions.

PACS numbers: 71.27.+a,71.10.Fd,71.30.+h,73.21.Ac,75.70.Cn

There is currently significant interest in understanding the electronic properties of bilayer graphene (BLG), in particular the ground state at the charge neutrality point. Several experimental studies [1–8] hint to the formation of a symmetry broken state in BLG, but its actual nature remains ambiguous and is at the moment a highly debated topic. Symmetry breaking in BLG can arise due to thermal annealing-induced strain on suspended samples as well as external electric fields applied perpendicular to the BLG sheets. In the absence of such external perturbations, due to the finite density of states at the Fermi level in the free band limit, the electronic Coulomb interaction is expected to trigger a genuine electronic instability and drive BLG into a correlated ground state [9]. Possible candidate states that have been suggested [10–22] include an (layered) antiferromagnetic (AF) state, several topological states such as quantum anomalous Hall, quantum spin Hall (QSH) or quantum valley Hall states, all of which exhibit a finite bulk gap, as well as a gapless nematic state. While most recent experiments identified a finite excitation gap of a few meV emerging in BLG at low temperatures [5–8], the transport data in Ref. [4] have been interpreted towards the formation of a gapless, possibly nematic state. Within the currently inconclusive experimental situation, an AF state is considered a probable ground state [22–24] among the (gapfull) candidates and thus worth a more detailed examination. Furthermore, the validity of approximative approaches need to be tested against unbiased and numerically exact results.

Here, we explore the nature of this possible ground state by taking screened Coulomb interactions into account within a tight-binding approach for BLG via a Hubbard model description of the carbon π - electrons. In particular, since the neutrality point relates to half-filling

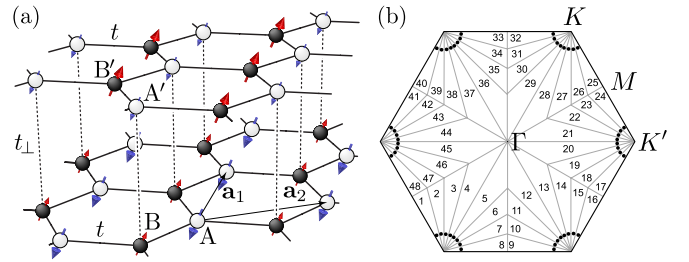


FIG. 1. (a) Bernal stacking of the honeycomb bilayer with intra- (inter)layer hopping t (t_{\perp}) between the sublattices A, B and A', B' (A', B). Within the sublattices an equal number of sites have a coordination number $z = 3$ or 4. (b) Patching scheme of the Brillouin zone in the fRG. Dots denote the momenta at which the vertex function is evaluated.

in the Hubbard model description, we take the opportunity to explore possible electronic instabilities using unbiased quantum Monte Carlo (QMC) methods. Our simulations are furthermore augmented by functional renormalization group (fRG) calculations [22, 25]. The fRG allows us to investigate the stability of the AF state obtained with QMC simulations over a broad range of the interaction strength. We find that within the AF ground state a local spin moment's participation in the AF order anticorrelates to its lattice coordination number z , with $z = 3$ or 4 for the Bernal stacking, an effect that we show to hold over the full parameter range from weak to strong electronic correlations.

In the following we consider the Hamiltonian $H = H_0 + H_{\text{int}}$, with the local interaction term $H_{\text{int}} = U \sum_i n_{i,\uparrow} n_{i,\downarrow}$ and $n_{i,\sigma} = c_{i,\sigma}^{\dagger} c_{i,\sigma}$ the density operator at site i for spin σ . Furthermore, H_0 denotes the free tight-binding model [9] containing both intralayer nearest neighbor

hopping t as well as interlayer hopping t_{\perp} , as illustrated in Fig. 1(a). For the onsite interaction U and also a finite set of nonlocal density-density interaction parameters, *ab initio* calculations list values for graphene and graphite [26], which have been used to explore the phase diagram of the honeycomb bilayer by means of the fRG approach that is also employed in the present work [22]. It was found that AF order is the dominant instability for interaction parameters with a shorter range than those for single layer graphene. As for a Bernal-stacked bilayer, where screening is expected to be effective, the antiferromagnet seems to be a viable candidate for the ground state of BLG. In this Letter, we employed an improved fRG patching of the Brillouin zone into 48 sectors, cf. Fig. 1(b), in order to obtain more accurate estimates for the critical energy scale Λ_c where an electronic instability emerges during the fRG flow while successively integrating out the high-energy modes. Details on the fRG approach have been presented in Ref. 22. From analyzing the structure of the resulting interaction vertex, we can identify the leading instability below Λ_c for varying sets of initial coupling parameters [25]. For a broad range of pure Hubbard interactions U , we observe a flow to strong coupling with the signature of an AF instability and an exponential dependence of Λ_c on U as discussed below. Up to an order of magnitude, Λ_c can serve as estimate for the single particle gap Δ_{sp} in the AF state. The AF instability is robust with respect to variations of the band structure, in particular the interlayer coupling, which we have explicitly checked for $t_{\perp} = 0.1t$ and $t_{\perp} = t$ (for BLG $t_{\perp} \approx 0.13t$ [27]). We take this as further motivation for a systematic analysis of the local Hubbard model at half-filling.

Our main findings result from analyzing this local Hubbard limit, where we can efficiently employ a projector QMC approach [28], to perform a numerically exact evaluation of the ground state properties. We furthermore fix $t_{\perp} = t$; while this takes us beyond the regime of realistic parameters for BLG, the choice for t_{\perp} allows us to reliably study electronic instabilities, due to the well pronounced quadratic band touching at the Fermi level [29]. We performed QMC simulations on finite systems of linear extent L (the number of sites being $N = 4L^2$) for L up to 12 with periodic boundary conditions. Our implementation also allows for the efficient measurement of unequal-time correlation functions [30]. From a fit of the imaginary-time displaced Green's function $G(\mathbf{q}, \tau) = \langle \frac{1}{N} \sum_{s,\sigma} c_{\mathbf{q}s\sigma}^{\dagger}(\tau) c_{\mathbf{q}s\sigma} \rangle$ to its long-time behavior, $\lim_{\tau \rightarrow \infty} G(\mathbf{q}, \tau) \propto e^{-\tau \Delta_{\text{sp}}(\mathbf{q})}$, the single-particle gap $\Delta_{\text{sp}} = \Delta_{\text{sp}}(K)$ can be extracted without the need of an analytical continuation. Here, s labels the four orbitals per unit cell of the honeycomb bilayer. In order to gain information on the influence of finite size (FS) effects we found it useful to compare also to fRG as well as to a AF mean-field theory (MFT) decoupling of the interaction term H_{int} . We

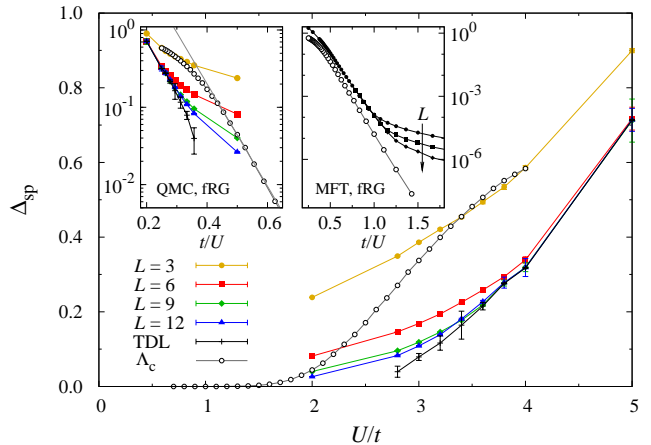


FIG. 2. Single particle gap Δ_{sp} from QMC simulations for different system sizes and the finite size extrapolation to the TDL using a polynomial fit function, along with the fRG critical scale Λ_c as a function of the local Coulomb repulsion U/t . The inset on the left shows the same data vs t/U in a semilog scale, exhibiting an exponential onset of the gap in the large t/U range. The inset on the right shows the fRG data along with MFT results for system sizes $L = 129, 258,$ and 516 .

solved the resulting saddle-point equations self consistently on finite lattices and zero temperature to obtain the MFT order parameters for the sublattice magnetization and the associated Hartree-Fock single particle gap $\Delta_{\text{sp}}^{\text{MFT}} = \min_{\{\mathbf{k}\}} \sqrt{\varepsilon(\mathbf{k})^2 + (Um)^2} = Um$, where $\varepsilon(\mathbf{k})$ the single particle dispersion of the free Hamiltonian H_0 .

In Fig. 2, we present our results for the single particle gap Δ_{sp} obtained from QMC simulations and MFT alongside the fRG critical scale Λ_c as a function of U/t . The QMC values exhibit a continuously increasing Δ_{sp} for all system sizes. The FS extrapolation to the thermodynamic limit (TDL) using a second order polynomial yields a continuous onset in the thermodynamic limit. Finite size extrapolation of the available data points deceptively suggest a finite critical value of U for the transition from the semimetal to the Mott insulator. We will show in the following that this can be attributed to pronounced FS effects at low energies. The fRG critical scale Λ_c (open circles) for the same parameters indeed reproduces such a continuously increasing associated single particle gap, for all finite values of U .

To identify whether the observed gap indeed is the consequence of a $U = 0^+$ instability, we plot Δ_{sp} as a function of t/U in the insets of Fig. 2. The fRG data show an exponential opening of Δ_{sp} in the large t/U regime (left inset). Accordingly, the FS extrapolated QMC data follow the same behavior. One can readily see that larger lattices are needed in order to clearly identify this exponential onset at smaller values of U/t . The same effect is observed already within the MF approach (right inset): increasingly larger system sizes allow us to identify the exponential opening of the single particle gap

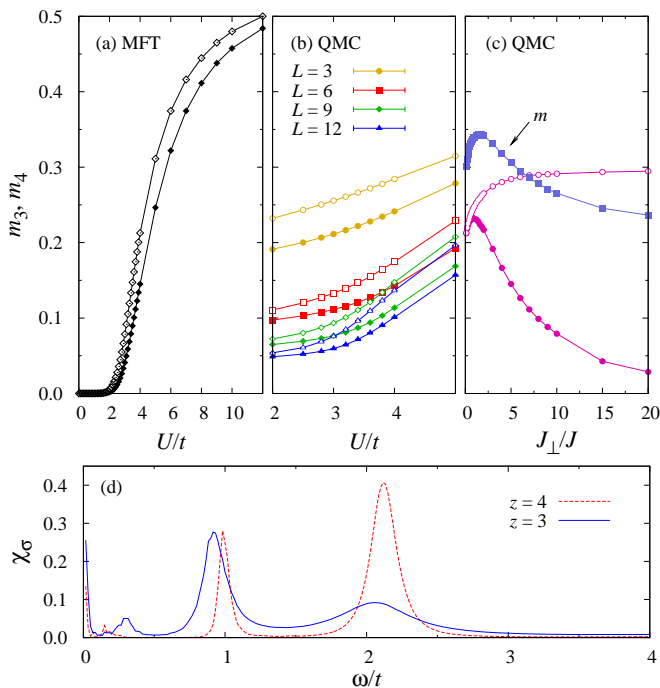


FIG. 3. The sublattice magnetization vs. U/t for sites with coordination number $z = 3$ (open symbols) and $z = 4$ (filled symbols) from (a) MFT in the TDL, (b) QMC simulations for different system sizes, and (c) in the Heisenberg limit vs. the interlayer AF exchange coupling J_{\perp}/J . The data in (c) result from SSE QMC simulations, after extrapolation to the TDL; also shown in (c) is the overall staggered magnetization m . Part (d) shows the local dynamical spin susceptibility $\chi_{\sigma}(\omega)$ for sites with $z = 3$ and 4 for $L = 12$, $U/t = 4$.

$\Delta_{\text{sp}} \propto \exp(-\alpha t/U)$. From our fRG data we can extract the exponent $\alpha \approx 16$, which is close to the Hartree-Fock value of $9\pi t^2/2t_{\perp}$ [31]. Deviations from this exponential behavior emerge beyond an intermediate coupling strength of $U/t \approx 2$ and relate to the onset of the strongly correlated regime. Note that within this model, the energy gap for realistic values of the Hubbard $U \approx 3t$ are rather large, $\Delta_{\text{sp}} \approx 0.07t \approx 200$ meV [26].

We identify the order parameter associated with the single particle gap from the low-energy vertex in the fRG and from corresponding correlation functions in QMC simulations, consistently, to be long-range AF order, correlated between both layers. To quantify this order within QMC simulations, we measure the overall staggered structure factor $S_{\text{AF}} = \frac{1}{N} \sum_{i,j} \epsilon_i \epsilon_j \langle \mathbf{S}_i \cdot \mathbf{S}_j \rangle$ from which we obtain the mean staggered magnetization per lattice site as $m = \sqrt{S_{\text{AF}}/(4L^2)}$. Here, $\epsilon_i = \pm 1$ if site i belongs to the magnetic sublattice A, A' (B, B'), as indicated by the white (black) spheres in Fig. 1. In order to probe in more detail the magnetic correlations, we also consider the following restricted structure factors for sites with coordination numbers $z = 3$ and 4 (for a system of linear size L , there are $2L^2$ such sites each):

$S_{\text{AF},z} = \frac{1}{2L^2} \sum_{i,j|z_i=z_j=z} \epsilon_i \epsilon_j \langle \mathbf{S}_i \cdot \mathbf{S}_j \rangle$ from which we obtain local order parameters $m_z = \sqrt{S_{\text{AF},z}/(2L^2)}$ for lattices sites with $z = 3, 4$. While the overall staggered magnetization m steadily increases with $U > 0$ like the single particle gap, we observe pronounced differences in the two sublattice magnetizations, which arise due to the presence of inequivalent sites in the lattice structure [cf. Fig. 3(a)-(b)]. In particular, we find that sites with the higher coordination $z = 4$ (filled symbols) exhibit a lower ordered moment, at odds with the usual intuition that high coordination favors more robust Néel order. An increase of z on one sublattice will generically make the ordering more robust everywhere, although not uniformly so for all sublattices. The same hierarchy of magnetic moments can also be inferred from fRG calculations for a wider range of nonlocal interactions by comparing the relative strengths of the effective interactions on the different sites of a unit cell.

Similar effects of an enhanced magnetic order near low-coordinated sites have previously been observed in localized quantum spin models on other inhomogeneous lattice structures [32]. Here, the joint bonds on sites with coordinated number $z = 4$ interconnect the two layers [cf. Fig. 1 (a)]. With increasing interaction U and hopping t_{\perp} , the moments along these bonds hybridize between the layers and tend to form spin singlets, suppressing the participation in the long range AF order on these sites. In Fig. 3(c), we consider the staggered magnetizations in the large- U limit, wherein the model becomes a spin-only Heisenberg model, with an intralayer exchange coupling $J = 4t^2/U$ and an interlayer coupling $J_{\perp} = 4t_{\perp}^2/U$. To study this Heisenberg limit of the Hubbard model, we employed the stochastic series expansion (SSE) QMC approach [33, 34], and present our results after an extrapolation to the TDL. We find that all three order parameters exhibit an initial increase upon increasing J_{\perp}/J . Furthermore, while m_3 saturates for large J_{\perp}/J , m and m_4 scale to zero in the large J_{\perp} limit. These results show that for all finite values of J/J_{\perp} , the system remains antiferromagnetically ordered, but with a suppressed staggered moment on the $z = 4$ sites for large J_{\perp}/J , due to the strong tendency towards forming J_{\perp} -singlets along these interlayer bonds. If the two honeycomb lattices were stacked such that each lattice site would be coupled via J_{\perp} to the other layer, a complete decoupling into local singlets would destroy the AF order beyond a finite critical value of J_{\perp}/J .

Returning to the Hubbard model, the local dynamical spin susceptibility $\chi_{\sigma,i}(\omega) = \sum_n |\langle n | S_i^x | 0 \rangle|^2 \delta(E_n - E_0 - \omega)$ also exhibits defined differences depending on the local coordination, cf. the QMC data in Fig. 3(d). While the peak near $\omega = 0$, related to the Goldstone mode in the TDL, is shared by both types of sites, the $z = 4$ sites exhibit a considerable shift of the residual spectral weight to larger energies as compared to the $z = 3$ sites, in ac-

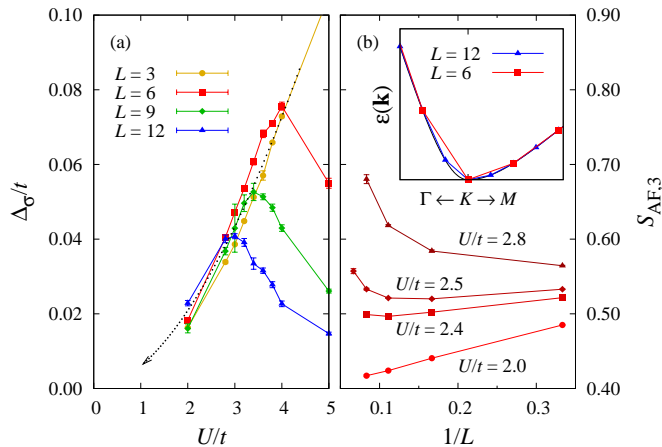


FIG. 4. Finite size behavior of (a) the spin gap Δ_σ and (b) the AF structure factor $S_{\text{AF},3}$ on lattice sites with coordination number $z = 3$. The inset in (b) illustrates the discretization effects on the free dispersion relation, a dominant source of finite size effects.

cordance with the associated reduced magnetic moment for $z = 4$.

To explore the global spin dynamical properties, Fig. 4(a) shows the spin gap Δ_σ from QMC simulations as a function of U/t for different system sizes (we obtain Δ_σ from the time-displaced spin-spin correlation function in the AF sector, $S_{\text{AF}}(\tau) = \frac{1}{N} \sum_{i,j} \epsilon_i \epsilon_j (\mathbf{S}_i(\tau) \cdot \mathbf{S}_j)$). The data for finite lattices exhibits a pronounced peak at intermediate values of U/t ; for increasingly larger lattice sizes, the position of this spin-gap dome shifts towards lower values of U/t , and its magnitude decreases, suggesting that in the TDL the spin gap vanishes for all values of U/t . While this is consistent with the emergence of Goldstone modes which originate in the spontaneous breaking of the $\text{SU}(2)$ spin symmetry in the AF phase, it furthermore illustrates the pronounced FS effects on the accessible range of system sizes. Similarly distinct FS corrections are also evident in the AF structure factor $S_{\text{AF},3}$, shown vs. $1/L$ in Fig. 4(b). Consider, for example, the data for $U/t = 2.4$: the initial downscaling of $S_{\text{AF},3}$ on small lattice sizes would suggest a magnetically disordered state. However, at larger lattice sizes the scaling behavior changes, and eventually a strong increase of $S_{\text{AF},3}$ with system size accounts for the formation of long-range AF order in the TDL. This peculiar FS scaling in fact arises both in the QMC simulations and the MFT order parameters (not shown). The FS effects become more pronounced for smaller t_\perp . The data in Fig. 4(b) also show that the corresponding crossover length scale beyond which the eventual increase of $S_{\text{AF},3}$ sets in, increases with decreasing values of U/t . Finite lattices, i.e., momentum space discretization, introduce a corresponding artificial gap which acts as a cutoff for correlations — an issue which afflicts all finite lattice simulations. When

dealing with a Fermi surface instability as in the present case, this generic FS effect becomes predominant on the accessible system sizes. The inset of Fig. 4(b) illustrates this discretization of the free dispersion around the Fermi level. Only for sufficiently large lattices will the parabolic band be approximated to such an extent as to probe the TDL nonlinear low energy dispersion.

In conclusion, we found from quantum Monte Carlo simulations, that the Hubbard model on the Bernal-stacked honeycomb bilayer as a basic model for BLG is prone to a Fermi point instability, which triggers layered AF order. Characterized by their different coordination numbers, sublattice sites sustain different magnetic moments. This peculiar local structure of the AF state relates to its stability in the strong interlayer tunneling region. A full quenching of the magnetic moments on the $z = 4$ sites emerges only in the (unrealistic) strong interlayer coupling limit and would eventually realize the layered AF state observed within chiral two-band models for bilayer graphene. Functional renormalization group calculations support the stability of the AF state and its moment distribution over a wide range of coupling parameters. In case the experimental support for a gapped state in BLG will be substantiated, it might be interesting to search for such an inhomogeneous AF state by local moment-sensitive probes such as magnetic scanning tunneling microscopy.

We thank S. Blügel, M. J. Schmidt, O. Vafek, T. Wehling, and F. Zhang for valuable discussions. This research was supported in part by the DFG research units FOR 723, 912, and 1162 and the NSF EPSCoR Cooperative Agreement No. EPS-1003897 with additional support from the Louisiana Board of Regents. Furthermore, we acknowledge the JSC Jülich and the HLRS Stuttgart for the allocation of CPU time.

* lang@physik.rwth-aachen.de

- [1] B. E. Feldman, J. Martin, A. Yacoby, *Nature Phys.* **5**, 889 (2009).
- [2] J. Martin, B. E. Feldman, R. T. Weitz, M. T. Allen, and A. Yacoby, *Phys. Rev. Lett.* **105** 256806 (2010).
- [3] R. T. Weitz, *et al.*, *Science* **330**, 812 (2010).
- [4] A. S. Mayorov *et al.*, *Science* **333**, 860 (2011).
- [5] F. Freitag, J. Trbovic, M. Weiss, and C. Schonenberger, *Phys. Rev. Lett.* **108**, 076602 (2012).
- [6] J. Velasco Jr. *et al.*, *Nat. Nanotechnol.* **7**, 156 (2012).
- [7] W. Bao *et al.*, *Proc. Natl. Acad. Sci. U.S.A.* **109**, 10802 (2012).
- [8] A. Veligura *et al.*, *Phys. Rev. B* **85**, 155412 (2012).
- [9] A. H. Castro Neto *et al.*, *Rev. Mod. Phys.* **81**, 109 (2009).
- [10] J. Nilsson, A. H. Castro Neto, N. M. R. Peres, and F. Guinea, *Phys. Rev. B* **73**, 214418 (2006).
- [11] E. McCann, D. S. L. Abergel, and V. I. Fal'ko, *Solid State Commun.* **143**, 110 (2007).
- [12] H. Min, G. Borghi, M. Polini, and A. H. MacDonald,

- Phys. Rev. B **77**, 041407 (2008).
- [13] Y. Lemonik, I. L. Aleiner, C. Toke, and V. I. Fal'ko, Phys. Rev. B **82**, 201408 (2010); Y. Lemonik, I. L. Aleiner, and V. I. Fal'ko, Phys. Rev. B **85**, 245451 (2012).
- [14] O. Vafek and K. Yang, Phys. Rev. B **81**, 041401 (2010).
- [15] R. Nandkishore and L. Levitov, Phys. Rev. Lett. **104**, 156803 (2010); Phys. Rev. B **82**, 115124 (2010).
- [16] F. Zhang, H. Min, M. Polini, and A. H. MacDonald, Phys. Rev. B **81**, 041402 (2010); A. H. MacDonald, J. Jung, and F. Zhang, Phys. Scr. 014012, (2012).
- [17] J. Jung, F. Zhang and A. H. MacDonald, Phys. Rev. B **83**, 115408 (2011); F. Zhang, J. Jung, G. A. Fiete, Q. Niu, and A. H. MacDonald, Phys. Rev. Lett. **106**, 156801 (2011).
- [18] O. Vafek, Phys. Rev. B **82**, 205106 (2010).
- [19] R. E. Throckmorton and O. Vafek, arXiv:1111.2076.
- [20] M. Kharitonov, arXiv:1109.1553.
- [21] V. N. Kotov *et al.*, Rev. Mod. Phys. **84**, 1067 (2012).
- [22] M. M. Scherer, S. Uebelacker, and C. Honerkamp, Phys. Rev. B **85**, 235408 (2012).
- [23] E. V. Gorbar *et al.*, arXiv:1204.2286.
- [24] F. Zhang, H. Min, and A. H. MacDonald, arXiv:1205.5532.
- [25] W. Metzner *et al.*, Rev. Mod. Phys. **84**, 299 (2012).
- [26] T. O. Wehling *et al.*, Phys. Rev. Lett. **106**, 236805 (2011).
- [27] L. M. Zhang *et al.*, Phys. Rev. B **78**, 235408 (2008).
- [28] F. F. Assaad and H. G. Evertz, Lect. Notes Phys. **739**, 277 (2008).
- [29] We use a trial wave function $|\Psi_T\rangle = \prod_{\sigma} |\Psi_T\rangle_{\sigma}$, where $|\Psi_T\rangle_{\sigma}$ is the ground state of the single particle Hamiltonian $H_{\sigma}^0 = -t \sum_{\langle i,j \rangle} c_{i\sigma}^{\dagger} c_{j\sigma} \exp\left(\frac{2\pi i}{\Phi_0} \int_{\mathbf{r}_i}^{\mathbf{r}_j} d\ell \cdot \mathbf{A}\right) + \text{H.c.}$ in the spin σ Hilbert subspace, where $\Phi_0 = he/c$ denotes the flux quantum, and \mathbf{r}_i the position of lattice site i . The flux $\Phi/\Phi_0 = 10^{-5}$ is chosen sufficiently small such that it is negligible within the achieved numerical accuracy to lift the ground state degeneracy in $|\Psi_T\rangle$. We employed a projection parameter $\Theta t = 50$ and an imaginary time discretization of $\Delta\tau t = 0.025$.
- [30] M. Feldbacher and F. F. Assaad, Phys. Rev. B **63**, 073105 (2001).
- [31] F. Gebhard, *The Mott Metal-Insulator Transition* (Springer, Berlin Heidelberg, 1997).
- [32] A. Jagannathan, R. Moessner, and S. Wessel, Phys. Rev. B **74**, 184410 (2006).
- [33] A. W. Sandvik, Phys. Rev. B **59**, R14157 (1999); O. F. Syljuåsen and A. W. Sandvik, Phys. Rev. E **66**, 046701 (2002).
- [34] The SSE results have been obtained from finite size simulations with $L = 6, 12, 18, 24$ at temperatures (couplings) $\beta/J = 6L$ representative for the ground state and their consecutive linear extrapolation to the TDL.